Mechanism of large production rates of α particles in reactions involving weakly bound projectiles

Arati Chavan [1] S. Rathi [1,*] K. Mahata [2,3] S. K. Pandit [2,3] V. V. Parkar [2,3] A. Shrivastava [2,3] K. Ramachandran [2]
A. M. Moro [4] H. Liu [5] Jin Lei [5] Sangeeta Dhuri [2,3,†] Satbir Kaur [2,3] Prasanna M. [6,‡] and Vineet Kumar [2,3]

[1] *Department of Physics, Vivekanand Education Society's College of Arts, Science and Commerce (Autonomous), Mumbai 400071, India*
[2] *Nuclear Physics Division, Bhabha Atomic Research Centre, Mumbai 400085, India*
[3] *Homi Bhabha National Institute, Anushaktinagar, Mumbai 400094, India*
[4] *Departamento de Física Atómica, Molecular y Nuclear, Facultad de Física, Universidad de Sevilla, Apartado 1065, Sevilla E-41080, Spain*
[5] *School of Physics Science and Engineering, Tongji University, Shanghai 200092, China*
[6] *Department of Physics, Rani Channamma University, Belagavi 591156, India*

(Received 9 January 2026; revised 3 April 2026; accepted 27 May 2026; published 25 June 2026)

To investigate the mechanism of α-particle production, energy-angle correlations of the emitted α particles have been measured for the $^{6}Li + ^{93}Nb$ system at energies around the Coulomb barrier. Results of three-body Monte Carlo simulations for breakup are in good agreement with the measured experimental energy-angle correlations. This is in contrast to the observation involving ^{7}Li projectile, where breakup simulation failed to reproduce the experimental data. Comparison of the data with two different semiclassical prescriptions for the optimum Q value leads to conflicting results, so no firm conclusion could be extracted from this comparison. Instead, fully quantum-mechanical calculations, employing the continuum-discretized coupled-channels (CDCC) method for the elastic breakup component and the Ichimura-Austern-Vincent (IAV) for the nonelastic one, reproduce the present experimental data rather well. The present study highlights the complexity of weakly bound projectile interactions and emphasizes the importance of more such studies for a comprehensive understanding.

DOI: 10.1103/6n73-4rb7

I. INTRODUCTION

Reactions with weakly bound stable/radioactive nuclei and the influence of breakup on elastic scattering and other reaction channels have received a great amount of attention in nuclear physics in recent years [1–5]. In addition to weak binding, nuclei away from the β-stability line exhibit exotic excitations and features like extended matter distribution, neutron skin, etc. Reaction studies with these nuclei are essential for modeling of nuclear reactions relevant to nuclear structure, reaction mechanisms, and nuclear astrophysics [6]. Due to limited availability and quality of radioactive ion beams, one can study the effect of weak binding with stable weakly bound nuclei very precisely and develop models to understand the role of other exotic features [7–14].

Stable weakly bound nuclei like $^{6,7}Li$, ^{9}Be have breakup threshold energies less than 2.5 MeV, much lower than the usual average binding per nucleon of 8 MeV for stable nuclei. Various inclusive and exclusive breakup studies have been performed with these stable weakly bound nuclei [15–34]. Reactions with weakly bound α-cluster nuclei are characterized by large α yields compared to the complementary fragment, suppression of complete fusion, and a commensurating incomplete fusion, indicating common underlying mechanism(s) [5,15,16,18,19,35]. However, the mechanisms and their relative importance have not been determined unambiguously. The yield of noncapture breakup, where both fragments escape, was found to be small compared to the total α yield. Thus, breakup fusion and cluster transfer are considered to be the main contributors of the above observations. Because the end products are the same, it is difficult to distinguish these two processes experimentally. Theoretical distinction is also not very clear. In many theoretical studies breakup fusion is treated as transfer to the continuum [36–38]. As the measured α energy distributions are often observed to peak around an energy that corresponds to the velocity of the elastically scattered particle, many studies have concluded the dominance of breakup-fusion mechanism. In a recent work [39], a novel proposition was put forward to distinguish between cluster transfer and breakup fusion. In case of one-step cluster transfer, the reaction Q value is shared among the ejected fragment (α particle) and the recoiling targetlike nuclei. However, in case of two-step breakup fusion, the ejected fragment produced in the first step should not have access to the Q value of the complementary fragment capture by the target nuclei in the second step. Based on this logic, it was shown that a sizable portion of the measured α spectra for $^{7}Li + ^{93}Nb$ reaction was not accessible to the breakup-fusion process. Further, the comparison of the

*Contact author: sarla.rathi@ves.ac.in
†Present address: Extreme Light Infrastructure - Nuclear Physics, IFIN-HH, 30 Reactorului Street, 077125 Magurele, Romania.
‡Present address: Department of Physics, Government First Grade College, Honnavara 581334, India.

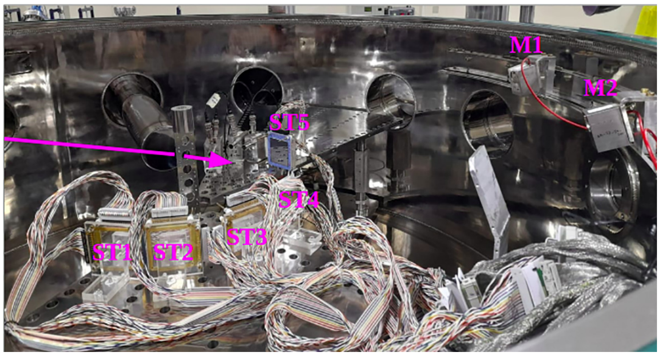

FIG. 1. Photograph of the experimental setup showing five segmented Si strip-detector telescopes (ST1–ST5), and two SSB detectors (M1, M2) used for beam monitoring and absolute normalization.

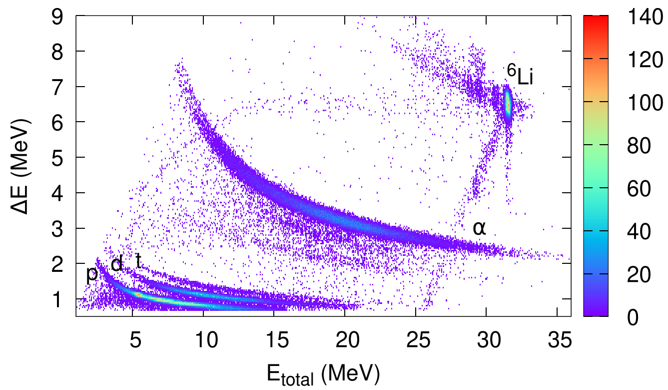

FIG. 2. Typical particle identification spectrum of ΔE vs E_{tot} for $^{6}\mathrm{Li} + {}^{93}\mathrm{Nb}$ at $E_{\mathrm{beam}} = 35$ MeV and $\theta_{\mathrm{lab}} = 56^{\circ}$.

experimental energy-angle correlations with results of three-body breakup simulation, transfer calculation using semi-classical and distorted-wave Born approximation (DWBA) approaches has clearly demonstrated the dominance of cluster transfer in the large production of α particle and incomplete fusion in that reaction. Similar observation was also reported for the $^{7}\mathrm{Li} + {}^{209}\mathrm{Bi}$ system [40]. These studies, involving in both cases ^{7}Li as projectile, have demonstrated that energy-angle correlations constitute a powerful tool to pin down the underlying reaction mechanisms. However, there are no such studies for ^{6}Li, which has a breakup threshold significantly lower than that of ^{7}Li. More studies with various projectile-target combinations are required to understand the intricate nature of the interactions involving weakly bound projectiles.

In this article, we present the results of energy-angle correlations of emitted α particles over a wide angular range in reaction of ^{6}Li with ^{93}Nb target at energies around the Coulomb barrier. To elucidate the nature of the underlying reaction mechanisms, the experimental data are compared with kinematical calculations for transfer, three-body Monte Carlo simulations for breakup, and quantum-mechanical calculations based on the inclusive breakup model of Ichimura, Austern, and Vincent (IAV).

II. EXPERIMENTAL DETAILS

The experiment was performed at the BARC-TIFR Pelletron LINAC Facility (PLF), Mumbai, by bombarding ^{6}Li beam of energies 25 and 35 MeV on self-supporting ^{93}Nb foil of thickness ≈ 2 mg/cm^{2} in a 1.5-m diameter general purpose scattering chamber. Energy-loss corrections are made at half the target thickness for both beam energies. Typical beam current, which was recorded using high-precision current integrator, was about 10 nA. The experimental setup consisted of 10 Si strip detectors (Micron Semiconductors) arranged as telescopes (ST1–ST5) along with two silicon surface-barrier (SSB) detectors (M1, M2). A photograph of the experimental setup is shown in Fig. 1. Si strip-detectors telescopes (ST1–ST5) are of active area 5×5 cm^{2} (thicknesses $\Delta E \approx 30$–50 μm, $E \approx 1.0$–1.5 mm). Four of these telescopes were placed on one arm and one detector telescope along with three Si surface-barrier detector telescopes placed on the other arm for measurements of charged particles. ΔE detectors were single sided with 16 strips on the front face which were aligned vertically with respect to beam direction, the E detectors were double sided with 16 strips each on the front and rear faces aligned horizontally and vertically, respectively. Width of each strip is 3.14 mm. The strip-detector telescopes, each having approximate angular coverage $\pm 8^{\circ}$, were mounted at angles 35°, 55°, 85°, 105°, and -55° at a distance of 18.5 cm from the target. Two Si-surface barrier detectors (thicknesses 300 μm) kept at $\pm 20^{\circ}$ were used to monitor Rutherford scattering. The data were collected in an event-by-event mode, using a VME data acquisition system. The triggers for the strip telescopes (ST1–ST5) were taken from the Mesytec make MSCF16 modules of the E detectors, which correspond to "OR" of all 16 strips. Final master gate was generated as the "OR" of the triggers from the strip telescopes, SSB (monitor) detectors. The detectors were calibrated using the known α energies from a ^{229}Th source and the $^{6}\mathrm{Li} + {}^{12}\mathrm{C}$ reaction at 25 MeV. Figure 2 represents typical ΔE vs E_{total} spectrum for 35-MeV beam energy for strip detector telescope 2 at 56°. As can be seen from Fig. 2, excellent particle identification could be achieved in the present measurement. The phenomenological analysis of the measured elastic-scattering angular distributions and the comparison of the measured inclusive α production cross sections with the literature data are published earlier [41].

III. RESULTS AND DISCUSSION

A. Energy-angle correlation of inclusive α particles

Measured energy-angle correlations are shown in Fig. 3. In order to interpret the experimental results, a Monte Carlo simulation code incorporating three-body kinematics was developed. The code, which was validated by reproducing the simulated data for ^{7}Li projectile [39], was used to calculate the energy-angle correlations of α particles from breakup for the present case. Emission of the ejectile in the laboratory frame and the fragments in the ejectile rest frame were assumed to be isotropic. The scattered energy of the ejectile was calculated using kinematics taking into account the Q value of the reaction and the excitation energies of the target as well as the ejectile. The excitation energy of the ejectile or the relative

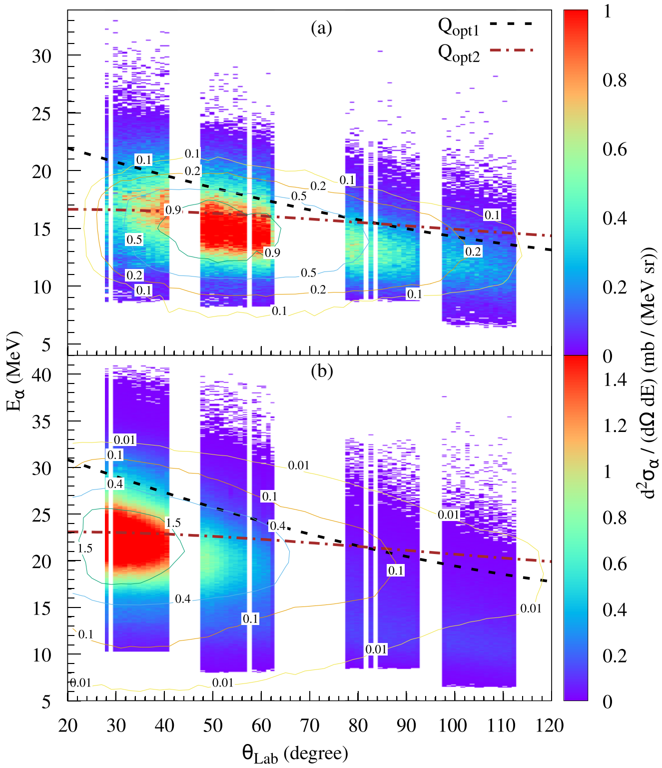

FIG. 3. Measured energy-angle correlation spectrum of inclusive α particles in the ^{6}Li + ^{93}Nb at (a) $E_{\text{lab}} = 24.6$ MeV and (b) $E_{\text{lab}} = 34.7$ MeV. Colored contours are results of breakup simulation. Energy-angle correlation spectrum is compared with kinematical line calculated using optimum Q value (Q_{opt1} [42] and Q_{opt2} [43]) (see text for more details).

energy (E_{rel}) of the fragments was randomly chosen according to the available experimental E_{rel} spectrum [26]. Energy and momentum conservations were used to obtain velocities of the fragments in the ejectile rest frame. Fragment velocities in laboratory frame, vector sum of fragment velocity in the ejectile rest frame, and ejectile velocity in the laboratory frame were used to calculate the energy and emission angle of the fragments in the laboratory frame. The simulated α-particle energy-angular distributions were normalized to match the simulated energy-integrated angular distributions to the experimental distributions (Fig. 6) at each angle. The measured energy-angle correlation spectra of inclusive α particles are compared with the results of the simulations (contours) and kinematical line using optimum Q value (Q_{opt1}) in Fig. 3. The semiclassical calculations of Q_{opt1} are based on Schiffer's prescription [42]. The value of "d" (difference in the distance of the closest approach in the initial and final trajectories) was taken as 1 fm based on the estimated shift of the center of mass before and after the transfer. The results are found to be less sensitive to the choice of d. When the value of d is changed by 0.5 fm (50%), value of E_α was found to change by $\approx 1.5\%$ at forward angle (35°) and $\approx 6\%$ at backward angle (105°). Another kinematical line (Q_{opt2}) is calculated using the optimum Q value derived from Brink's matching conditions for transfer [43], assuming that the transfer process

TABLE I. The breakup threshold (E_{th}) and d/t-transfer Q value are compared.

Projectile	E_{th} (MeV)	Target	Q value for d/t-transfer (MeV)
^{6}Li	1.47	^{93}Nb	12.16
		^{209}Bi	5.84
^{7}Li	2.47	^{93}Nb	14.06
		^{209}Bi	4.59

takes place at the distance of closest approach for a Coulomb classical trajectory for each scattering angle. The optimal Q value becomes a function of the scattering angle.

As can be seen in Fig. 3, the experimental energy-angle correlations match well with the breakup simulation in the case of the ^{6}Li + ^{93}Nb reaction, whereas they do not match with the kinematical line calculated using the optimum Q value (Q_{opt1}) based on Schiffer's prescription. By contrast, the kinematical line calculated with Brink's formula (Q_{opt2}) explains the data quite well. In the case of the ^{7}Li + ^{93}Nb reaction [39], the experimental energy-angle correlation was in good agreement with the transfer calculation, but differed significantly from the simulated distribution from breakup process. It should be noted that good agreement between the experimental data in case of ^{7}Li projectile [39,40] and the results of kinematic calculations based on Schiffer's prescription was considered as a signature of dominance of cluster transfer. However, the present study indicates that the simple kinematical calculations may not be sufficient to identify the underlying reaction mechanism.

The above observation highlights the strong dependence of the reaction mechanism on the projectile in reactions involving weakly bound projectiles. The breakup threshold and the d (t)-transfer Q values for ^{6,7}Li projectiles with ^{93}Nb and ^{209}Bi are compared in Table I. In the case of the reactions induced by ^{7}Li on ^{93}Nb and ^{209}Bi targets, the difference in t-transfer Q value is very large. However, in both cases the dominance of cluster transfer was observed. Thus, the breakup threshold might play a crucial role rather than the transfer Q value in deciding the reaction pathways.

B. Quantum-mechanical analysis of elastic scattering and α-particle production

In this section, we present fully quantum-mechanical calculations for the elastic scattering and inclusive α-particle production in the ^{6}Li + ^{93}Nb system. We employ the continuum-discretized coupled-channels (CDCC) method [44] for the elastic breakup (EBU) component, in which ^{6}Li dissociates into $\alpha + d$ while the target remains in its ground state, and the Ichimura-Austern-Vincent (IAV) model [45] for the nonelastic breakup (NEB) component, in which the unobserved deuteron undergoes a nonelastic interaction with the target (absorption, transfer, etc.). Below, we first describe the theoretical framework and input parameters, then present detailed comparisons with the experimental data.

CDCC framework. The CDCC method provides a three-body quantum-mechanical description of the $\alpha + d + {}^{93}$Nb system by discretizing the α-d continuum into a finite set of bins. The calculations include s-wave ($J^\pi = 1^+$), p-wave ($J^\pi = 0^-, 1^-, 2^-$), and d-wave ($J^\pi = 1^+, 2^+, 3^+$) continuum states. For the d-wave states, we adopt a finer binning scheme to accurately capture the resonant states of ^{6}Li at excitation energies of 2.186 MeV ($J^\pi = 3^+$), 4.31 MeV ($J^\pi = 2^+$), and 5.7 MeV ($J^\pi = 1^+$). The $\alpha + d$ ground state is described using a Woods-Saxon potential with parameters $V_0 = 78.46$ MeV, $r_0 = 1.83$ fm, absolute radius $R = 3.32$ fm, and $a = 0.7$ fm [46]. For the p- and d-wave states, we use a modified Woods-Saxon potential with $V_0 = 80.0$ MeV, $r_0 = 1.83$ fm, $a = 0.7$ fm, supplemented with a spin-orbit term of the standard Woods-Saxon derivative form, featuring $V_{so} = 2.5$ MeV, $r_{so} = 1.83$ fm, and $a_{so} = 0.7$ fm, to properly position the d-wave resonances. The calculations employed the code FRESCO [47]. The CDCC calculation provides observables with respect to the excitation energy and center of mass of the projectile, which are then transformed to triple differential cross sections with respect to the angles and energies of the individual fragments (α and d) using the formalism and codes developed in Ref. [48].

For the fragment-target interactions, we utilize global optical-potential parameters for the $d + {}^{93}$Nb and $\alpha + {}^{93}$Nb systems from Refs. [49] and [50], respectively. This two-cluster ($\alpha + d$) model for ^{6}Li has been widely applied in CDCC calculations for various ^{6}Li-induced reactions. However, to achieve agreement with the elastic-scattering data, such calculations typically require a reduction in the imaginary part of the fragment-target interactions [21,51–53], to mitigate the overestimation of absorption effects inherent in the two-body approximation [54]. Accordingly, we reduce the surface term of the deuteron-target imaginary potential by half.

IAV model. For the NEB component, we employ the IAV model [45], which provides a quantum-mechanical framework for calculating inclusive breakup cross sections. In this formulation, the inclusive breakup process $a(=b + x) + A \to b + B^*$ is expressed in terms of the expectation value of the imaginary part of the x-A optical potential and a source term containing the entrance-channel wave function projected onto the internal states of the projectile and target [55]. Here b (α) is the observed fragment and x (d) is the unobserved one that undergoes any nonelastic process with the target. The present calculations employ the DWBA form of the IAV model [55–57], where the entrance-channel distorted wave is generated using the ^{6}Li + ^{93}Nb optical model potential. This is in contrast to the full CDCC-IAV formulation [58], in which the complete three-body CDCC wave function is used to describe the entrance channel. For weakly bound projectiles such as ^{6}Li, the DWBA form has been shown to approximate well the full CDCC-IAV results [58], thus justifying its use in the present analysis. The fragment-target optical potentials are kept the same as in the CDCC calculation for consistency. The ^{6}Li + ^{93}Nb entrance-channel interaction is modeled using the São Paulo potential (SPP) [59,60], with standard renormalization factors $N_R = 1.0$ and $N_I = 0.78$ for the real and imaginary parts, respectively. The spectroscopic factor (SF) for the $\alpha + d$ clustering in ^{6}Li is taken as SF = 0.83, consistent with the range 0.75–0.85 reported in Ref. [61]. The total inclusive breakup cross section for the observed α particle is then obtained as (NEB + EBU)×SF.

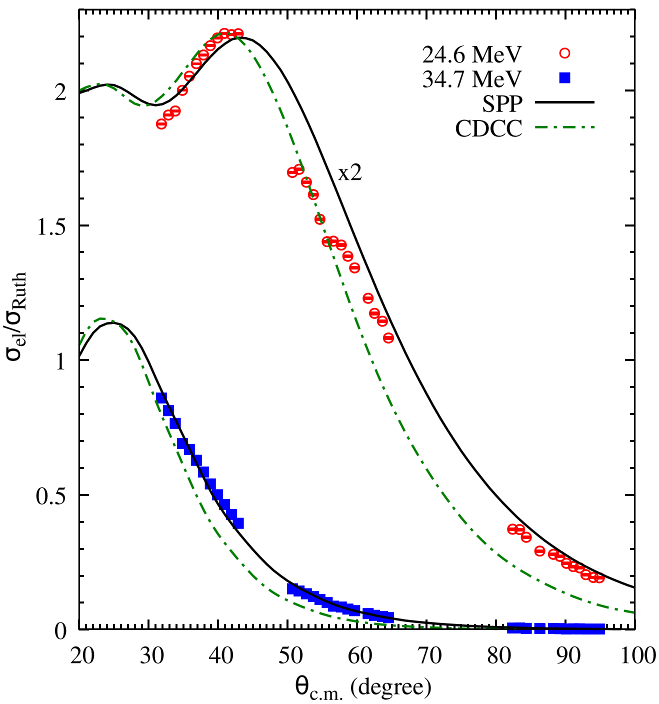

FIG. 4. Elastic-scattering angular distribution for ^{6}Li + ^{93}Nb at $E_{lab} = 24.6$ MeV and 34.7 MeV. Solid lines correspond to results of optical-model calculations using São Paulo potential (SPP), whereas dot-dashed lines correspond to continuum-discretized coupled-channels calculations (CDCC).

Elastic scattering. As a first test of the theoretical inputs, we compare the calculated elastic-scattering angular distributions with the experimental data. The measured elastic-scattering cross sections, normalized to the Rutherford cross sections, for ^{6}Li + ^{93}Nb at $E_{lab} = 24.6$ and 34.7 MeV are shown in Fig. 4. The measured angular distribution exhibits a peak around 43° for E_{lab}=24.6 MeV. In contrast, at $E_{lab} = 34.7$ MeV only the falling part of the distribution is observed within the measured angular range, with the Fresnel bump expected to appear at forward angles. To understand the measured angular distribution, two sets of calculations are performed, *viz.* SPP and CDCC calculations. The SPP calculation employs the double-folding São Paulo potential [59,60], which accounts for the effects of Pauli nonlocality. The CDCC calculation explicitly treats the coupling to the $\alpha + d$ breakup continuum as described above. Both calculations provide a satisfactory description of the elastic-scattering data over the measured angular range, exhibiting the characteristic Fresnel diffraction pattern with the rainbow angle shifting to more forward angles at the higher energy. The agreement between the two approaches indicates that the phenomenological SPP effectively captures the effects of breakup coupling on the elastic channel. This consistency gives confidence in the entrance-channel optical potential used for the IAV-DWBA calculation of the α production cross sections.

α-particle energy spectra. α particles can be produced in the laboratory through direct-reaction processes, such as

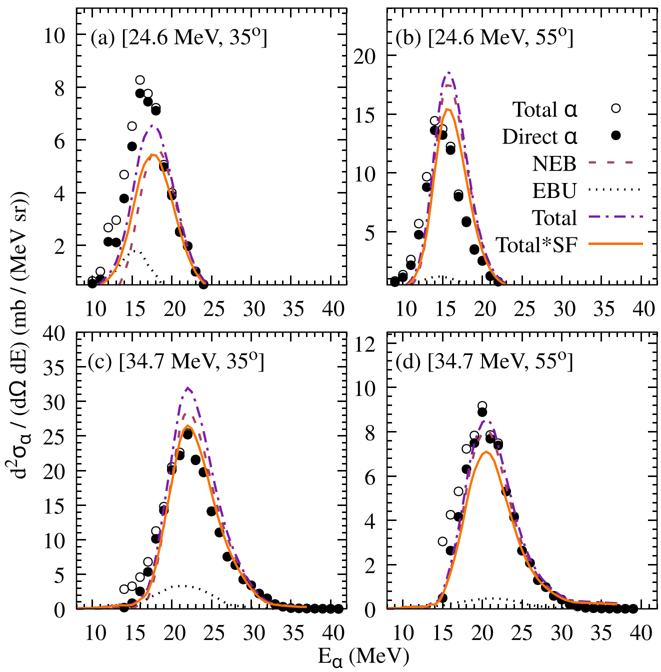

FIG. 5. Double differential cross sections as a function of the α-particle energy. Numbers in the square brackets represent $E_{\rm lab}$ and $\theta_{\rm lab}$. Open circles and filled circles correspond to the total α and direct α contributions, respectively. The dashed, dotted, dot-dashed, and solid lines correspond to results of Ichimura-Austern-Vincent (IAV) model calculation for nonelastic breakup (NEB), elastic breakup (EBU), total, and total$\times$SF calculations, respectively. SF is spectroscopic factor.

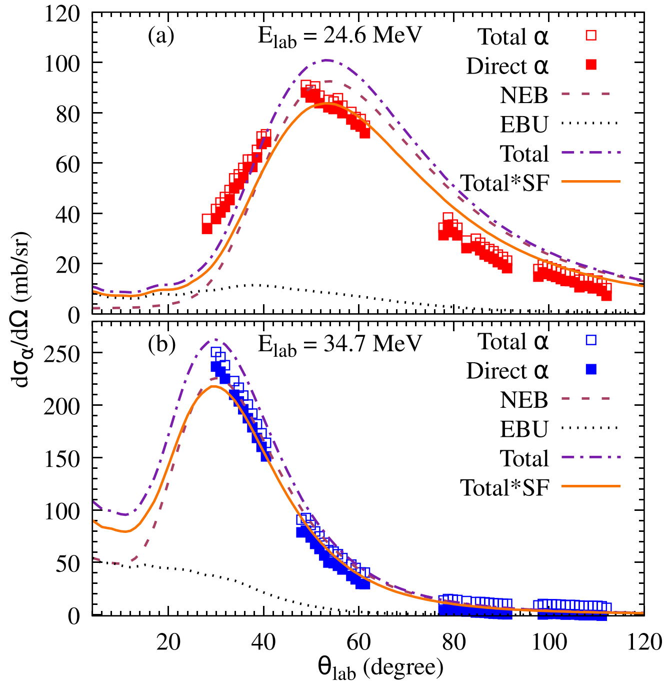

FIG. 6. α angular distribution for ^{6}Li + ^{93}Nb at $E_{\rm lab}$ = 24.6 MeV and 34.7 MeV. Open squares and filled squares correspond to the total α and direct α contributions, respectively. Statistical error bars are smaller than the symbol size and hence not shown. The dashed, dotted, dot-dashed, and solid lines correspond to the results of Ichimura-Austern-Vincent (IAV) model calculation for nonelastic breakup (NEB), elastic breakup (EBU), total, and total$\times$SF calculations, respectively. SF is spectroscopic factor.

breakup and transfer breakup, as well as through evaporation from the compound nucleus. The measured inclusive or total α energy spectra at representative laboratory angles for $E_{\rm lab} = 24.6$ and 34.7 MeV are shown in Fig. 5, along with the individual EBU and NEB contributions, their sum (NEB + EBU), and the total scaled by the spectroscopic factor (NEB + EBU)$\times$SF. In these plots, the direct α contributions are obtained by subtracting the estimated compound nuclear contributions from the measured total α contributions. More details about the statistical-model estimate of the compound nuclear contributions can be found in Ref. [41]. Several important features emerge from this comparison. First, the NEB component dominates over the EBU at both energies and all measured angles. It has been also reported that noncapture breakup, where both the fragments escape, is much smaller than the total α production [5,24,31]. This indicates that the α particles are predominantly produced through nonelastic processes in which the deuteron is absorbed by the target, consistent with the incomplete fusion picture. Second, the peak position of the calculated α energy spectrum agrees well with the experimental data, occurring near the energy corresponding to beam-velocity α particles, which supports the breakup origin of the direct α yield. Third, the overall magnitude and shape of the inclusive α energy spectra are well reproduced by theoretical calculation, particularly at forward angles where the breakup mechanism is expected to dominate. At backward angles and at the higher beam energy ($E_{\rm lab} = 34.7$ MeV), the calculations tend to slightly underestimate the data, which may suggest contributions from processes not included in the present two-body breakup framework, such as multistep reactions and due to limitations/uncertainties of the underlying ingredients, such as pairwise interactions entering the CDCC and IAV calculations.

α-particle angular distribution. The angle-integrated α-particle cross sections at both energies are compared with the calculations in Fig. 6. The measured inclusive α data and the calculated NEB, EBU, NEB + EBU, and (NEB + EBU)$\times$SF contributions are shown. The measured angular distributions exhibit a forward-peaked shape characteristic of direct-reaction processes. The NEB component is the dominant contribution at all angles, exceeding the EBU by approximately an order of magnitude, further confirming the predominance of nonelastic breakup in α production. The calculated (NEB + EBU)$\times$SF provides a good overall description of the inclusive α angular distribution at both energies, successfully reproducing the forward peaking and the angular dependence. At $E_{\rm lab} = 24.6$ MeV, the agreement is particularly good across the entire angular range, while at $E_{\rm lab} = 34.7$ MeV some underestimation is observed at the most backward angles, consistent with the trend observed in the energy spectra.

Model comparison and implications. The CDCC+IAV-DWBA calculations successfully reproduce the main features of the measured α production in the ^{6}Li + ^{93}Nb system, including the energy spectra, angular distributions, and absolute cross sections with the spectroscopic factor SF = 0.83. The dominance of NEB over EBU establishes that the α particles predominantly arise from nonelastic breakup, in which the deuteron is captured by the target. This provides quantitative support for the breakup origin of the large α yield observed in ^{6}Li-induced reactions at near-barrier energies.These quantum-mechanical results are also consistent with the three-body Monte Carlo breakup simulation discussed in Sec. III A. While the simulation validates the kinematics of the emitted α particles against the breakup scenario, the CDCC + IAV calculations provide a more complete, first-principles description including both the EBU and NEB components with absolute cross sections. The mutual agreement between these two complementary approaches strengthens the conclusion that breakup (elastic and nonelastic) is the dominant mechanism for α production in the $^{6}\text{Li} + {}^{93}\text{Nb}$ system. However, the present analysis also reveals limitations. The slight underestimation at backward angles and higher energy suggests possible inaccuracies of the underlying potentials, limitations of the adopted reaction models, or the presence of additional processes beyond the inclusive two-body breakup framework, such as multistep mechanisms or other processes beyond the inclusive two-body breakup picture. Furthermore, the use of a single spectroscopic factor to scale both EBU and NEB is an approximation; in principle these two components may have different sensitivities to the projectile structure. Nevertheless, the overall agreement supports the elastic and nonelastic breakup mechanism as the primary source of the observed α particles. It is instructive to contrast these findings with the $^{7}\text{Li} + {}^{93}\text{Nb}$ system [39], where direct cluster (triton) stripping was identified as the dominant mechanism for α production. Despite the similar α-cluster structure of ^{6,7}Li and comparable transfer Q values (Table I), the measured energy-angle correlation of ^{6,7}Li on ^{93}Nb are found to be different. This difference can be attributed to the lower breakup threshold of ^{6}Li (1.47 MeV) compared to ^{7}Li (2.47 MeV), which favors the breakup channel in the former case. These findings underscore the sensitivity of the reaction mechanism to the projectile binding energy and highlight the need for fully quantum-mechanical analyses, rather than simple semiclassical prescriptions, to reliably identify the dominant processes in reactions involving weakly bound nuclei.

IV. SUMMARY AND CONCLUSION

In summary, energy-angle correlations of the emitted α particles have been measured in $^{6}\text{Li} + {}^{93}\text{Nb}$ system at energies around the Coulomb barrier. Monte Carlo simulation using three-body kinematics considering direct and sequential breakup have been carried out to investigate the mechanism of α-particle production. The measured experimental energy-angle correlations are found to be in good agreement with the three-body Monte Carlo simulations for breakup. Comparison of the measured energy-angle correlations were found to be consistent by Brink's optimal kinematical conditions for transfer [43], assuming that the transfer takes place at the distance of closest approach for each scattering angle. By contrast, comparison with Schiffer's prescription [42] showed a larger departure from the data, particularly at the smaller scattering angles. This is in contrast to the observation in $^{7}\text{Li} + {}^{93}\text{Nb}$ reaction, where the experimental data was found to agree well with the kinematic line based on Schiffer's prescription, and differ significantly from the results of breakup simulation. It would be interesting to investigate the energy-angle correlations with a high-Z target like ^{209}Bi with ^{6}Li projectile as similar variation in d-cluster transfer Q value is also present in that case. Quantum-mechanical calculations based on the CDCC method (for the elastic breakup) and the Ichimura-Austern-Vincent (IAV) DWBA model (for the nonelastic breakup) were found to reproduce the present experimental results rather well. The present study highlights the complexity of weakly bound projectile interactions and emphasizes the importance of more study for a comprehensive understanding.

ACKNOWLEDGMENTS

We thank PLF accelerator staff, Mumbai, for providing steady and uninterrupted beam and also Mr. A. Kumar and Mr. P. Patle for help during the experiment. Two of the authors (A.C. and S.R.) would like to acknowledge the funding from University Grants Commission Department of Atomic Energy Consortium for Scientific Research Kolkata Centre (UGC-DAE-CSR-KC), India (Grants No. CRS/19/NP06/0917, No. 0502, No. 0391, and No. 0202). A.M.M. acknowledges funding from Grants No. PID2020-114687GB-I00 and No. PID2023-146401NB-I00 by MICIU/AEI/10.13039/501100011033.

DATA AVAILABILITY

The data that support the findings of this article are not publicly available upon publication because it is not technically feasible and/or the cost of preparing, depositing, and hosting the data would be prohibitive within the terms of this research project. The data are available from the authors upon reasonable request.

[1] L. F. Canto, P. R. S. Gomes, R. Donangelo, and M. S. Hussein, Fusion and breakup of weakly bound nuclei, Phys. Rep. **424**, 1 (2006).

[2] N. Keeley, R. Raabe, N. Alamanos, and J. L. Sida, Fusion and direct reactions of halo nuclei at energies around the Coulomb barrier, Prog. Part. Nucl. Phys. **59**, 579 (2007).

[3] N. Keeley, N. Alamanos, K. W. Kemper, and K. Rusek, Elastic scattering and reactions of light exotic beams, Prog. Part. Nucl. Phys. **63**, 396 (2009).

[4] L. F. Canto, P. R. S. Gomes, R. Donangelo, J. Lubian, and M. S. Hussein, Recent developments in fusion and direct reactions with weakly bound nuclei, Phys. Rep. **596**, 1 (2015).

[5] V. Jha, V. V. Parkar, and S. Kailas, Incomplete fusion reactions using strongly and weakly bound projectiles, Phys. Rep. **845**, 1 (2020).
[6] C. Bertulani and T. Kajino, Frontiers in nuclear astrophysics, Prog. Part. Nucl. Phys. **89**, 56 (2016).
[7] J. Lei and A. M. Moro, Unraveling the reaction mechanisms leading to partial fusion of weakly bound nuclei, Phys. Rev. Lett. **123**, 232501 (2019).
[8] J. Lei and A. M. Moro, Puzzle of complete fusion suppression in weakly bound nuclei: A Trojan Horse effect? Phys. Rev. Lett. **122**, 042503 (2019).
[9] J. Rangel, M. R. Cortes, J. Lubian, and L. F. Canto, Theory of complete and incomplete fusion of weakly bound systems, Phys. Lett. B **803**, 135337 (2020).
[10] A. Diaz-Torres, D. J. Hinde, J. A. Tostevin, M. Dasgupta, and L. R. Gasques, Relating breakup and incomplete fusion of weakly bound nuclei through a classical trajectory model with stochastic breakup, Phys. Rev. Lett. **98**, 152701 (2007).
[11] V. V. Parkar, V. Jha, and S. Kailas, Exploring contributions from incomplete fusion in ^{6,7}Li + ^{209}Bi and ^{6,7}Li + ^{198}Pt reactions, Phys. Rev. C **94**, 024609 (2016).
[12] G. Potel, F. M. Nunes, and I. J. Thompson, Establishing a theory for deuteron-induced surrogate reactions, Phys. Rev. C **92**, 034611 (2015).
[13] I. J. Thompson and A. Diaz-Torres, Modelling effects of halo breakup on fusion, Prog. Theor. Phys. Suppl. **154**, 69 (2004).
[14] R. Shyam, G. Baur, and P. Banerjee, Projectile breakup by nuclear and Coulomb fields and application to astrophysically relevant radiative-capture processes, Phys. Rev. C **44**, 915 (1991).
[15] K. Pfeiffer, E. Speth, and K. Bethge, Break-up of ^{6}Li and ^{7}Li on tin and nickel nuclei, Nucl. Phys. A **206**, 545 (1973).
[16] R. Ost, K. Bethge, H. Gemmeke, L. Lassen, and D. Scholz, Three-particle correlations from ^{208}Pb + ^{6}Li, Z. Phys. **266**, 369 (1974).
[17] H. Utsunomiya, S. Kubono, M. H. Tanaka, M. Sugitani, K. Morita, T. Nomura, and Y. Hamajima, Breakup fusion of ^{7}Li, Phys. Rev. C **28**, 1975 (1983).
[18] C. M. Castaneda, H. A. Smith, P. P. Singh, and H. Karwowski, Mechanisms of production of fast particles with $Z = 1, 2$ in ^{6}Li -induced reactions far above the Coulomb barrier, Phys. Rev. C **21**, 179 (1980).
[19] C. Signorini, A. Edifizi, M. Mazzocco, M. Lunardon, D. Fabris, A. Vitturi, P. Scopel, F. Soramel, L. Stroe, G. Prete, E. Fioretto, M. Cinausero, M. Trotta, A. Brondi, R. Moro, G. L. Rana, E. Vardaci, A. Ordine, G. Inglima, M. L. Commara, *et al.*, Exclusive breakup of ^{6}Li by ^{208}Pb at Coulomb barrier energies, Phys. Rev. C **67**, 044607 (2003).
[20] A. Shrivastava, A. Navin, N. Keeley, K. Mahata, K. Ramachandran, V. Nanal, V. V. Parkar, A. Chatterjee, and S. Kailas, Evidence for transfer followed by breakup in ^{7}Li + ^{65}Cu, Phys. Lett. B **633**, 463 (2006).
[21] S. Santra, V. V. Parkar, K. Ramachandran, U. K. Pal, A. Shrivastava, B. J. Roy, B. K. Nayak, A. Chatterjee, R. K. Choudhury, and S. Kailas, Resonant breakup of ^{6}Li by ^{209}Bi, Phys. Lett. B **677**, 139 (2009).
[22] S. Santra, S. Kailas, V. V. Parkar, K. Ramachandran, V. Jha, A. Chatterjee, P. K. Rath, and A. Parihari, Disentangling reaction mechanisms for α production in the ^{6}Li + ^{209}Bi reaction, Phys. Rev. C **85**, 014612 (2012).
[23] A. Pakou, O. Sgouros, V. Soukeras, J. Casal, and K. Rusek, Reaction mechanisms of the weakly bound nuclei ^{6,7}Li and ^{7,9}Be on light targets at near barrier energies, Eur. Phys. J. A **58**, 8 (2022).
[24] S. K. Pandit, A. Shrivastava, K. Mahata, N. Keeley, V. V. Parkar, P. C. Rout, K. Ramachandran, I. Martel, C. S. Palshetkar, A. Kumar, A. Chatterjee, and S. Kailas, Probing transfer to unbound states of the ejectile with weakly bound ^{7}Li on ^{93}Nb, Phys. Rev. C **93**, 061602(R) (2016).
[25] S. K. Pandit, A. Shrivastava, K. Mahata, V. V. Parkar, N. Keeley, P. C. Rout, K. Ramachandran, C. S. Palshetkar, I. Martel, A. Kumar, A. Chatterjee, and S. Kailas, Role of target shell structure in direct reactions involving weakly bound ^{7}Li, Phys. Rev. C **100**, 014618 (2019).
[26] D. Luong, M. Dasgupta, D. Hinde, R. du Rietz, R. Rafiei, C. Lin, M. Evers, and A. Diaz-Torres, Insights into the mechanisms and time-scales of breakup of ^{6,7}Li, Phys. Lett. B **695**, 105 (2011).
[27] H. Kumawat, V. Jha, V. V. Parkar, B. J. Roy, S. Santra, V. Kumar, D. Dutta, P. Shukla, L. M. Pant, A. K. Mohanty, R. K. Choudhury, and S. Kailas, Inclusive α -production cross section for the ^{6}Li + ^{90}Zr system at energies near the fusion barrier, Phys. Rev. C **81**, 054601 (2010).
[28] B. R. Fulton, R. L. Cowin, R. J. Woolliscroft, N. M. Clarke, L. Donadille, M. Freer, P. J. Leask, S. M. Singer, M. P. Nicoli, B. Benoit, F. Hanappe, A. Ninane, N. A. Orr, J. Tillier, and L. Stuttgé, Exclusive breakup measurements for ^{9}Be, Phys. Rev. C **70**, 047602 (2004).
[29] R. Rafiei, R. du Rietz, D. H. Luong, D. J. Hinde, M. Dasgupta, M. Evers, and A. Diaz-Torres, Mechanisms and systematics of breakup in reactions of ^{9}Be at near-barrier energies, Phys. Rev. C **81**, 024601 (2010).
[30] C. S. Palshetkar, S. Santra, A. Shrivastava, A. Chatterjee, S. K. Pandit, K. Ramachandran, V. V. Parkar, V. Nanal, V. Jha, B. J. Roy, and S. Kalias, Elastic scattering and α production in the ^{9}Be + ^{89}Y system, Phys. Rev. C **89**, 064610 (2014).
[31] D. Chattopadhyay, S. Santra, A. Pal, A. Kundu, K. Ramachandran, R. Tripathi, D. Sarkar, S. Sodaye, B. K. Nayak, A. Saxena, and S. Kailas, Resonant, direct, and transfer breakup of ^{6}Li by ^{112}Sn, Phys. Rev. C **94**, 061602(R) (2016).
[32] K. J. Cook, E. C. Simpson, D. H. Luong, S. Kalkal, M. Dasgupta, and D. J. Hinde, Importance of lifetime effects in breakup and suppression of complete fusion in reactions of weakly bound nuclei, Phys. Rev. C **93**, 064604 (2016).
[33] S. Kaur, S. K. Pandit, V. V. Parkar, A. Shrivastava, K. Mahata, K. Ramachandran, S. Dhuri, Prasanna M., P. C. Rout, and S. Gupta, Breakup and neutron stripping in the ^{9}Be + ^{124}Sn system from α-α coincidence measurement, Phys. Rev. C **111**, 054603 (2025).
[34] T. Singh, S. Santra, A. Baishya, A. Pal, P. C. Rout, R. Gandhi, A. Kundu, D. Chattopadhyay, and R. Tripathi, One-neutron stripping followed by breakup of ^{9}Be in the field of ^{209}Bi, Phys. Rev. C **111**, 054615 (2025).
[35] V. V. Parkar, V. Jha, and S. Kailas, Systematics and mechanisms of α production with weakly and strongly bound projectiles, Eur. Phys. J. A **59**, 88 (2023).
[36] G. Baur and D. Trautmann, The break-up of the deuteron and stripping to unbound states, Phys. Rep. **25**, 293 (1976).
[37] A. Bonaccorso and D. M. Brink, Absorption versus breakup in heavy-ion reactions, Phys. Rev. C **43**, 299 (1991).

[38] A. M. Moro and F. M. Nunes, Transfer to the continuum and breakup reactions, Nucl. Phys. A **767**, 138 (2006).

[39] S. K. Pandit, A. Shrivastava, K. Mahata, N. Keeley, V. V. Parkar, R. Palit, P. C. Rout, K. Ramachandran, A. Kumar, S. Bhattacharyya, V. Nanal, S. Biswas, S. Saha, J. Sethi, P. Singh, and S. Kailas, Unraveling the reaction mechanism for large alpha production and incomplete fusion in reactions involving weakly bound stable nuclei, Phys. Lett. B **820**, 136570 (2021).

[40] K. J. Cook, E. C. Simpson, L. T. Bezzina, M. Dasgupta, D. J. Hinde, K. Banerjee, A. C. Berriman, and C. Sengupta, Origins of incomplete fusion products and the suppression of complete fusion in reactions of ^{7}Li, Phys. Rev. Lett. **122**, 102501 (2019).

[41] A. Chavan, S. Rathi, K. Mahata, S. K. Pandit, V. V. Parkar, A. Shrivastava, K. Ramachandran, S. Dhuri, S. Kaur, Prasanna M., and V. Kumar, Elastic scattering and inclusive α angular distributions for ^{6}Li + ^{93}Nb system around the Coulomb barrier, Nucl. Phys. A **1067**, 123303 (2026).

[42] J. Schiffer, H. Körner, R. Siemssen, K. Jones, and A. Schwarzschild, Experimental study of angular distributions and optimum Q values in heavy-ion reactions, Phys. Lett. B **44**, 47 (1973).

[43] D. Brink, Kinematical effects in heavy-ion reactions, Phys. Lett. B **40**, 37 (1972).

[44] N. Austern, Y. Iseri, M. Kamimura, M. Kawai, G. Rawitscher, and M. Yahiro, Continuum-discretized coupled-channels calculations for three-body models of deuteron-nucleus reactions, Phys. Rep. **154**, 125 (1987).

[45] M. Ichimura, N. Austern, and C. M. Vincent, Equivalence of post and prior sum rules for inclusive breakup reactions, Phys. Rev. C **32**, 431 (1985).

[46] H. Nishioka, J. Tostevin, R. Johnson, and K.-I. Kubo, Projectile excitation and structure effects in ^{6}Li and ^{7}Li scattering, Nucl. Phys. A **415**, 230 (1984).

[47] I. J. Thompson, Coupled reaction channels calculations in nuclear physics, Comput. Phys. Rep. **7**, 167 (1988).

[48] J. A. Tostevin, F. M. Nunes, and I. J. Thompson, Calculations of three-body observables in ^{8}B breakup, Phys. Rev. C **63**, 024617 (2001).

[49] H. An and C. Cai, Global deuteron optical model potential for the energy range up to 183 MeV, Phys. Rev. C **73**, 054605 (2006).

[50] V. Avrigeanu, P. E. Hodgson, and M. Avrigeanu, Global optical potentials for emitted alpha particles, Phys. Rev. C **49**, 2136 (1994).

[51] Y. Hirabayashi and Y. Sakuragi, Anomalous renormalization of cluster-folding interactions for ^{6}Li-nucleus scattering at low energies, Phys. Lett. B **258**, 11 (1991).

[52] C. Beck, N. Keeley, and A. Diaz-Torres, Coupled-channel effects in elastic scattering and near-barrier fusion induced by weakly bound nuclei and exotic halo nuclei, Phys. Rev. C **75**, 054605 (2007).

[53] J. Lei and A. M. Moro, Comprehensive analysis of large α yields observed in ^{6}Li -induced reactions, Phys. Rev. C **95**, 044605 (2017).

[54] S. Watanabe, T. Matsumoto, K. Minomo, K. Ogata, and M. Yahiro, Effects of four-body breakup on ^{6}Li elastic scattering near the Coulomb barrier, Phys. Rev. C **86**, 031601(R) (2012).

[55] J. Lei and A. M. Moro, Reexamining closed-form formulae for inclusive breakup: Application to deuteron- and ^{6}Li -induced reactions, Phys. Rev. C **92**, 044616 (2015).

[56] J. Lei, Inclusive breakup calculations in angular momentum basis: Application to ^{7}Li + ^{58}Ni, Phys. Rev. C **97**, 034628 (2018).

[57] J. Lei and P. Descouvemont, Lagrange-mesh *R* -matrix method for inhomogeneous equations, Phys. Rev. C **102**, 014608 (2020).

[58] J. Lei and A. M. Moro, Advancing the Ichimura-Austern-Vincent model with continuum-discretized coupled-channels wave functions for realistic descriptions of two-body projectile breakup, Phys. Rev. C **108**, 034612 (2023).

[59] L. C. Chamon, B. V. Carlson, L. R. Gasques, D. Pereira, C. D. Conti, M. A. G. Alvarez, M. S. Hussein, M. A. C. Ribeiro, E. S. Rossi, and C. P. Silva, Toward a global description of the nucleus-nucleus interaction, Phys. Rev. C **66**, 014610 (2002).

[60] M. Alvarez, L. Chamon, M. Hussein, D. Pereira, L. Gasques, E. Rossi, and C. Silva, A parameter-free optical potential for the heavy-ion elastic scattering process, Nucl. Phys. A **723**, 93 (2003).

[61] T. Yoshimura, A. Okihana, R. Warner, N. Chant, P. Roos, C. Samanta, S. Kakigi, N. Koori, M. Fujiwara, N. Matsuoka, K. Tamura, E. Kubo, and K. Ushiro, Alpha spectroscopic factors for ^{6}Li, ^{7}Li, ^{9}Be and ^{12}C from the (p, pα) reaction at 296 MeV, Nucl. Phys. A **641**, 3 (1998).